Mechanisms of nonequilibrium electron-phonon coupling and thermal conductance at interfaces

Ashutosh Giri, John T. Gaskins, Brian F. Donovan, Chester Szwejkowski, Ronald J. Warzoha, Mark A. Rodriguez, Jon Ihlefeld, and Patrick E. Hopkins

Citation: Journal of Applied Physics **117**, 105105 (2015); doi: 10.1063/1.4914867
View online: http://dx.doi.org/10.1063/1.4914867
View Table of Contents: http://scitation.aip.org/content/aip/journal/jap/117/10?ver=pdfcov
Published by the AIP Publishing

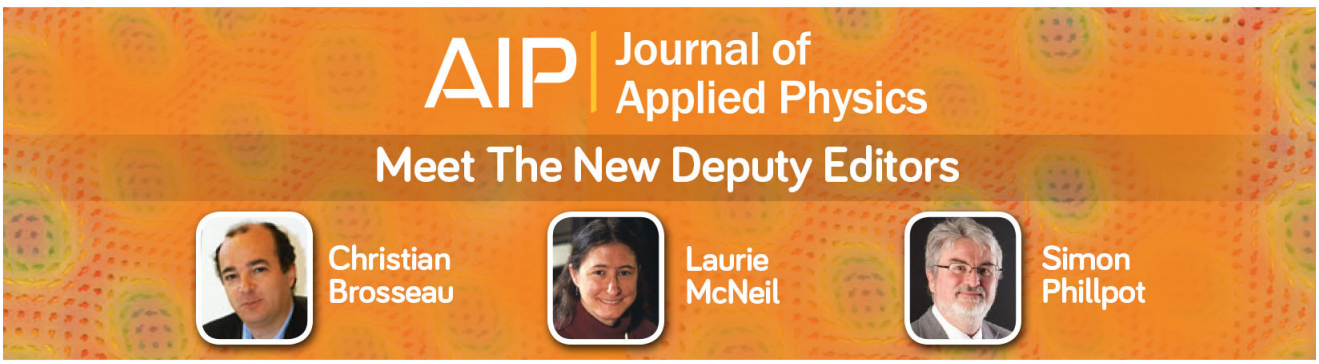

Mechanisms of nonequilibrium electron-phonon coupling and thermal conductance at interfaces

Ashutosh Giri,[1] John T. Gaskins,[1] Brian F. Donovan,[1] Chester Szwejkowski,[1] Ronald J. Warzoha,[2] Mark A. Rodriguez,[3] Jon Ihlefeld,[3] and Patrick E. Hopkins[1,a)]
[1]*Department of Mechanical and Aerospace Engineering, University of Virginia, Charlottesville, Virginia 22904, USA*
[2]*Department of Mechanical Engineering, United States Naval Academy, Annapolis, Maryland 21401, USA*
[3]*Sandia National Laboratories, Albuquerque, New Mexico 87123, USA*

(Received 14 January 2015; accepted 2 March 2015; published online 13 March 2015)

We study the electron and phonon thermal coupling mechanisms at interfaces between gold films with and without Ti adhesion layers on various substrates via pump-probe time-domain thermoreflectance. The coupling between the electronic and the vibrational states is increased by more than a factor of five with the inclusion of an ~3 nm Ti adhesion layer between the Au film and the nonmetal substrate. Furthermore, we show an increase in the rate of relaxation of the electron system with increasing electron and lattice temperatures induced by the laser power and attribute this to enhanced electron-electron scattering, a transport channel that becomes more pronounced with increased electron temperatures. The inclusion of the Ti layer also results in a linear dependence of the electron-phonon relaxation rate with temperature, which we attribute to the coupling of electrons at and near the Ti/substrate interface. This enhanced electron-phonon coupling due to electron-interface scattering is shown to have negligible influence on the Kapitza conductances between the Au/Ti and the substrates at longer time scales when the electrons and phonons in the metal have equilibrated. These results suggest that only during highly nonequilibrium conditions between the electrons and phonons ($T_e \gg T_p$) does electron-phonon scattering at an interface contribute to thermal boundary conductance. © *2015 AIP Publishing LLC*. [http://dx.doi.org/10.1063/1.4914867]

I. INTRODUCTION

Nonequilibrium dynamics within and between the electronic and vibrational states in solids govern a variety of phenomena in materials physics. For example, the weak coupling between these two states is known to limit thermal transport in various metals, such as Au and Cu.[1–3] The volumetric transfer of energy between these two energetic states is defined by the electron-phonon (e-p) coupling factor. This energy relaxation mechanism between the fundamental energy carriers has been studied for quantum dots,[4] nanorods[5] and more notably for homogenous metal films, which has been extensively studied through theoretical and experimental approaches.[3,6–14] Laser pulses with sub-picosecond resolution have been used to track the non-equilibrium thermal relaxation mechanisms of the metal films through traditional pump-probe techniques.[8,10,13,15,16] However, the fundamental scattering processes driving this energy transport are still unclear. For example, at elevated laser fluences, grain boundaries, lattice defects, and interfaces could play a significant role in the relaxation of the electron gas in the metal. In addition, we have recently shown that electron-electron (e-e) scattering can enhance the effective rate of e-p relaxation when the electrons are highly out of equilibrium with the surrounding lattice.[17]

The purpose of our current study is to investigate the electron energy transfer processes occurring at and near the film-substrate interfaces, and how these processes affect thermal transport at different time scales after short pulsed laser heating. Immediately after excitation with an ultrashort laser pulse, the electron gas in a metal can be heated to several thousand degrees above the lattice temperature due to the large differences in their specific heats. Pump-probe thermoreflectance measurements allow the capability to examine the Fermi relaxation dynamics, e-p relaxation as well as phonon-phonon thermalization processes by relating the change in reflectivity of the sample surface to various rate-relaxation models. For example, the e-p coupling factor, G, for a thin Au film on a dielectric substrate can be determined by fitting the initial rise and the fast transient decay of the TDTR signal in the first few picoseconds (as shown in Fig. 1) to the two-temperature model (TTM).[18] The e-p nonequilibrium dynamics also governs the generation and propagation of acoustic-phonon pulses[19,20] through the homogeneous thin film that is characterized by the oscillatory TDTR signal in the 10–100 ps time regime of Fig. 1. The longer pump-probe delay times of up to several nanoseconds are generally fitted by heat conduction model to back out thermal properties such as the thermal conductivities of the film and the substrate and the thermal boundary conductance (TBC).[21–23] In this work, we will analyze the different time scales represented in Fig. 1 for a series of Au films on various substrates. Specifically, we study the influence of interfacial properties on the rate of e-p equilibration and the effect of this initial relaxation process on the heat transport at different time scales in these nanosystems.

Typically, heat transport across metal/non-metal interfaces is found to be dominated by phonon-phonon scattering

a)Electronic mail: phopkins@virginia.edu

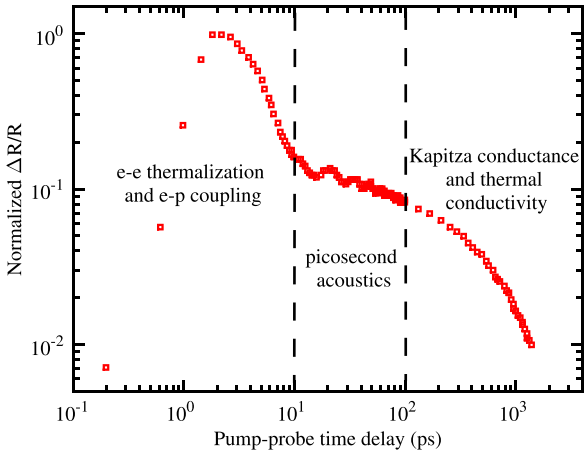

FIG. 1. Thermoreflectance signal for a 20 nm Au/Si sample plotted as a function of delay time between the pump and probe pulses. The data show three distinct time regimes; the initial 10 ps during and after laser pulse absorption that is characterized by electronic thermalization in the Au film, followed by the picosecond acoustics regime that is marked by the periodic oscillatory signal caused by longitudinal displacement of, or a strain wave propagation in the film and the final time scale where the signal decays due to heat transport across the film substrate interface and thermal effusion into the substrate. In this plot, 2 ps is arbitrarily chosen as the maximum signal. We note that for this particular data set, the cross correlation of the pump and probe pulses is ~700 fs.

processes.[24,25] However, there exist several experimental results that cannot be predicted by theoretical models that are solely based on phonon mediated transport such as the well known diffuse mismatch model and the acoustic mismatch model.[24,26,27] These works allude to the fact that the discrepancies in the theoretical models and the experimental results arise due to the exclusion of physics that account for metal electron to non-metal phonon interactions within the models. This led to more robust theoretical models from Huberman and Overhauser[28] and Sergeev[29,30] that proposed a different channel of energy transport across metal/dielectric interfaces.

Lyeo and Cahill[31] have shown that electron-interface scattering for Pb and Bi films on a diamond substrate does not enhance the thermal boundary conductance. Their results showed that the TBC is mainly driven by phonon scattering processes, as Pb and Bi, which have similar Debye temperatures yet different electron densities around their respective Fermi surfaces, have comparable TBCs across the metal/substrate interface. Their findings have been supported by various phonon-phonon scattering theories.[32–34] In addition, recently, Singh *et al.*[35] have shown that at non-cryogenic temperatures, metal-electrons exhibit an adiabatic boundary condition when scattering at metal/insulator interfaces. Indeed, the thermal boundary conductance across metal/substrate interfaces is primarily driven by phonons in the regime of moderate non-equilibrium conditions between electrons and phonons. This is in line with the hypothesis by Majumdar and Reddy[36] in which the electrons must first couple with the surrounding phonons in the metal film before phonons can carry heat across the interface.

Understanding the interfacial scattering mechanisms under conditions of strong non-equilibrium between electrons and phonons, however, has received far less attention. For example, we have previously shown that in thin gold films on rough Si substrates, the influence of interfacial roughness on e-p relaxation is only quantifiable at high effective electron temperatures.[17] Along these lines, we have shown both experimentally[37,38] and theoretically[39] that during conditions of both e-e and e-p nonequilibrium, the electron cooling dynamics after short pulsed excitation can in fact be influenced by the metal/substrate interface. Clearly, based on our previous works, under conditions of strong e-p nonequilibrium, electron energy exchange at or across a metal/non-metal interface can affect e-p equilibration and TBC. However, the phase space of this energy transport pathway, which exists only under strong nonequilibrium conditions, is relatively unchartered compared to its phonon-phonon counterpart.[40] Additionally, systematic studies to determine how interfacial properties of different, well characterized metal/substrate combinations can affect energy flow from a nonequilibrium electron gas are necessary to fortify our understanding of e-p dynamics in warm-dense electron systems.

In light of the discussions in the previous paragraphs, we measure the effective e-p coupling factor, G_{eff}, in Au films on various non-metal substrates with and without a very thin (~3 nm) Ti adhesion layer across a wide range of electron temperatures($T_e \sim 400$–2000 K). The thin Ti adhesion layer is deposited to not only enhance the bonding between the metal film and the dielectric substrate but also to provide a strong channel for electron-phonon energy exchange near the interface relative to the weak electron-phonon coupling characteristic of Au. The inclusion of the Ti adhesion layer is shown to significantly increase the measured G_{eff} of the Au/Ti films compared to a system without the adhesion layer. By repeating our measurements for three different non-metallic substrates with different thermal conductivities and phonon properties, we relate the electron-interface scattering to thermal boundary conductance and phonon properties of the substrate. We also show an increase in the G_{eff} values due to an increase in temperature, which is in contrast to the conventional e-p energy exchange theory based on free electrons[6] where the e-p coupling factor is independent of temperatures greater than the Debye temperature of the metal. We attribute this temperature dependence and increase in G_{eff} to the increase in the number of electronic states around the Fermi level that couple their energy to the lattice vibrations. Finally, we measure the TBC across metal/substrate interfaces with and without the Ti adhesion layer and show that at time scales when the electrons have fully thermalized with the phonons, the electron-interface conductance does not influence heat transport.

II. EXPERIMENTAL DETAILS

A. Sample preparation and characterization

Nominally 20 nm of gold films with and without a titanium adhesion layer were evaporated onto crystalline silicon, crystalline sapphire, and fused silica using electron-beam evaporation. Thickness of the heterostructures was measured via the X-ray reflectivity (XRR) technique, which was performed using a Scintag PAD X diffractometer equipped with

a sealed-tube Cu anode (goniometer radius = 240 mm). Generator settings were 40 kV and 30 mA. Monochromatic Cu Ka (0.15406 nm) radiation was generated through the use of an incident beam mirror optic. The mirror exit aperture was set to a height of 50 μm to ensure minimal beam loss at low angles (i.e., $< 0.5^\circ$ 2θ) so as to assure accurate critical edge determination. The diffraction system employed a Peltier-cooled Ge solid-state detector with a 0.2° receiving slit. XRR data were fit using the Software program *Parratt32* (Version 1.5.2) employing a two-layer (Au/Ti/substrate) model. The measured thicknesses are tabulated in Table I. Atomic force microscopy study conducted on all the samples exhibited high quality smooth surfaces with roughnesses less than 1 nm.

B. Experimental technique and data analysis

Our thermoreflectance measurements were carried out using the TDTR technique which has been explained in detail in Refs. 21–23. We use a mode:locked Ti:Sapphire laser that produces pulses centered at 800 nm at a repetition rate of 80 MHz. We use two wavelengths for the pump and probe beams where the former has been frequency doubled from 1.55 eV to 3.1 eV. The laser spot sizes were focused on to the sample surface through a 10× objective to $1/e^2$ radii values of 7.0 and 6.0 μm for pump and probe beams, respectively. The average probe power in our experiments was fixed at 9 mW, whereas the average pump power was adjusted between experiments from 5 mW to 60 mW to probe the effects of increasing e-p nonequilibrium. The absorption of the pump pulses by the sample surface leads to a rapid increase in the internal energy of the electron system, which then transfers its energy to the lattice vibrations. This provides a unique path forward to directly measure how electrons in various states of nonequilibrium interact with the surrounding vibrational environment in metal nanosystems. We monitor the change in the optical properties created due to this thermal relaxation process with the reflected probe beam at the frequency with which we modulate the pump beam in our experiment (8.8 MHz).

The temperature dynamics underlying the measured thermoreflectance data were determined using a modified TTM,[3,17] which takes into account the delay in the thermalization process of the electronic system. Due to the long life-times of the non-Fermi distribution of electrons at lower lattice and electron temperatures,[12,41] the modified TTM measures the "effective" electron temperatures for our measurements. The main aspect of the modified TTM that is relevant to the current work is its ability to account for a temporally lagging evolution of the electron energy density after pulse absorption, compared to the traditional TTM. The respective time evolution of the electron and lattice temperatures is given by

$$C_e(T_\mathrm{p})\frac{\partial T_{\mathrm{e,eff}}}{\partial t} = \nabla\cdot(\kappa_e\nabla T_{\mathrm{e,eff}}) - G_{\mathrm{eff}}(T_{\mathrm{e,eff}} - T_\mathrm{p}) + S(t),$$
$$C_p(T_\mathrm{p})\frac{\partial T_\mathrm{p}}{\partial t} = \nabla\cdot(\kappa_p\nabla T_p) + G_{\mathrm{eff}}(T_{\mathrm{e,eff}} - T_\mathrm{p}), \quad (1)$$

where C_e and C_p are the heat capacities of the electrons and phonons, respectively. Similarly, κ_e and κ_p are the thermal conductivities of the electrons and phonons, respectively, and $S(t)$ is the source term that is modified to account for the delayed relaxation in the electronic distribution.[3] Immediately after the pump pulses are incident on the sample surface, the highly non-equilibrium electrons absorb the photon energies and traverse the Au film thickness with velocities close to the Fermi velocity.[14] This ballistic nature of the "hot" electrons in our thin films creates a homogeneously heated thin film which simplifies the modified TTM by eliminating the electron and phonon diffusion terms during e-p equilibration. Note the parabolic two-step radiation model (Eq. (1)) that is used to analyze the data in this work assume infinite speeds of energy propagation,[42] which for our thin film samples are a valid approximation since there are no spatial gradients in the nonthermal distribution of the electrons. However, for thicker samples that are greater than the ballistic penetration depth of the electrons in Au, the hyperbolic two-step radiation heating model (as explained in Ref. 42) would be the more appropriate thermal model to analyze the TDTR data.

To determine the initial energy distribution in the multilayer films, we use the transfer matrix method[43] to calculate the light absorption as a function of space in the Au/Ti bi-layers. We use a mixing rule based on the percentage of light absorbed by the electron system in the bi-layers to calculate the material parameters in Eq. (1). The thicknesses of the bi-layers were measured via X-ray reflectivity measurements (and confirmed by mechanical profilometery) and are tabulated in Table I along with each of the essential material parameters required for the TTM. We note that even though Ti is not a free electron metal, the free electron approximation for electron heat capacity agrees well with heat capacity calculated using an *ab initio*-derived electron density of states.[44] It should also be noted that we cannot spatially discretize the thin films due to the fact that the thicknesses are less than the mean free path of e-p relaxation in the respective bilayers.

The relation between a metal's reflectivity and the complex dielectric function based on the Drude model is exploited in order to predict the effective electron and phonon temperatures from the thermoreflectance response.[47] We calculate the amount of laser energy absorbed by the

TABLE I. Parameters used in the thermoreflectance model for the Au/Ti/Si, Au/Ti/Al_2O_3, and Au/Ti/SiO_2 structures. γ_e is the electronic heat capacity coefficient in the TTM. The thicknesses of Au and Ti bi-layers were measured by X-ray reflectivity measurements.

	Au	Ti
C_p ($\times 10^6$ J m^{-3} K^{-1})	2.49[a]	3.01[b]
γ_e (J m^{-3} K^{-2})	62.9[c]	328.9[c]
d (nm) on Si substrate	16.1 ± 0.2	3.1 ± 0.2
d (nm) on Al_2O_3 substrate	16.2 ± 0.6	2.7 ± 0.2
d (nm) on SiO_2 substrate	15.7 ± 0.7	2.8 ± 0.7

[a]Reference 45.
[b]Reference 46.
[c]Reference 44.

electrons in the sample, according to the thin film optics approach explained in Refs. 48 and 49. We take precaution to make sure that the absorbed fluence does not increase the conduction band number density due to d-band excitations. This is because the Drude-based thermoreflectance model only takes into account the change in reflectivity due to intraband transitions.[50] The probe energy is well below the interband transition threshold for Au (2.4 eV) supporting our use of the aforementioned intraband thermoreflectance model. Even at the maximum absorbed laser fluence, we estimate that the conduction band number density will only be perturbed by <2%.[51] Note that the effective electron temperatures in our predictions from the modified TTM do not exceed 3000 K. Above this temperature, the conduction band number density is changed due to d-band transitions that cause a change in the chemical potential and occupied density of states, rendering the thermoreflectance model ineffective.[44,52] The thermoreflectance model requires the proper knowledge of the e-e and e-p collisional frequencies, which are $\nu_{ee} = A_{ee}T_e^2$ and $\nu_{ep} = B_{ep}T_p$, respectively.[50] In Ref. 17, we have shown a method by which the scattering coefficients can be calculated for any metallic nanosystem given relatively small perturbations of the electron temperature.

We analyze the magnitude of the thermoreflectance signal using the values of A_{ee} and B_{ep} determined for Au/Ti/Si, Au/Ti/Al_2O_3, and Au/Ti/SiO_2 systems. The thermoreflectance model is fit to the experimental data by normalizing the peak electron temperature to the peak in the reflectance signal while iterating G_{eff} until the minimum error between the model and the data are produced. Figure 2 compares the TDTR data and TTM fits for a 20.0 nm Au film on a fused silica substrate (red square) and a 15.7 nm Au/2.8 nm Ti on fused silica substrate (blue circle). The fast transient decay in the signal for Au/Ti/fused silica shows that the inclusion of the Ti adhesion layer significantly decreases the electron relaxation time and causes an increase in the measured G_{eff} values.

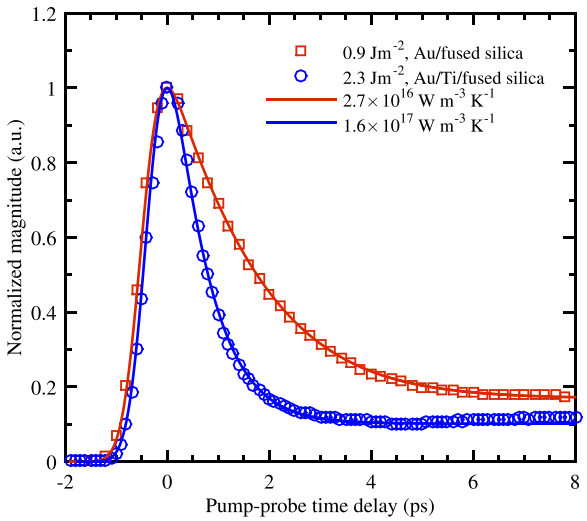

FIG. 2. TDTR data on Au/fused silica (red square) and Au/Ti/fused silica (blue circle) samples at room temperature and corresponding best fits using the modified TTM with a nonlinear thermoreflectance model.[17] The data are normalized by the maximum magnitude of the signal from the lock-in amplifier.

III. RESULTS AND DISCUSSION

A. Ballistic transport and electron scattering at the interface

Figure 3 shows the measured values of G_{eff} as a function of total temperature of the electronic and vibrational states in Au films with Ti adhesion layers on three substrates (sapphire, silicon and fused silica). We define total temperature as the sum of the maximum lattice and electron temperatures predicted via our TTM analysis. Due to the relatively lower thermal effusivities of the fused silica and sapphire substrates compared to that of silicon, there is an additional temperature rise in the metal which we refer to as DC heating, ΔT_{DC}. This temperature rise of the metal bi-layers can be estimated through the expression,[53]

$$\Delta T_{\text{DC}} = \frac{(1-R)\dot{q}}{k\left(2\pi\omega_0^2 + 2\pi\omega_1^2\right)^{1/2}}. \quad (2)$$

Here $\dot{q}$ is the incident laser power, R is the reflectivity, k is the thermal conductivity of the substrate, and ω_0 and ω_1 are pump and probe radii, respectively. Not accounting for this DC heating results in an under prediction of the rate of e-p relaxation.[17]

For comparison, Fig. 3 also plots the G_{eff} values for samples without the Ti layer. The agreement between the measured G_{eff} for these samples suggests that the mechanisms driving e-p relaxation are intrinsic to Au films and independent of the Si and fused silica substrates along with the interfacial region between the Au and the substrate. However, with the inclusion of the thin Ti layer, the dependency of G_{eff} on the substrate becomes prominent and the G_{eff} increases by as much as five fold in the electron temperature

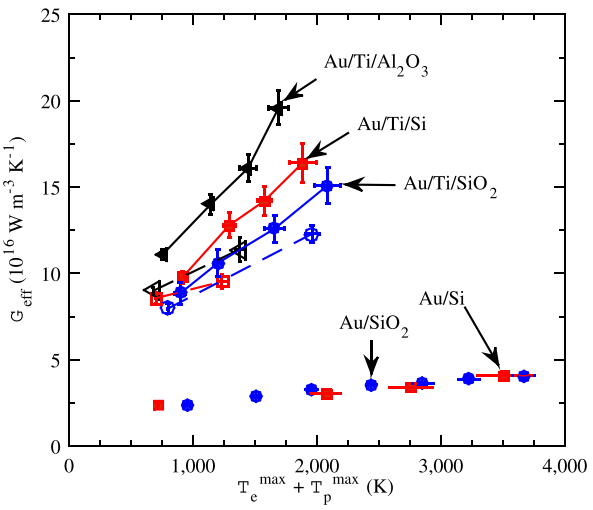

FIG. 3. G_{eff} as a function of maximum effective electron temperature plus maximum phonon temperature from DC laser heating for Au/Ti/fused silica (blue circle), Au/Ti/Si (red square), and Au/Ti/sapphire (black triangle). For comparison, we have also plotted G_{eff} values for Au/Si and Au/fused silica. The hollow symbols represent data for Au films with a thickness of 40 nm with Ti adhesion layer on different substrates. After accounting for ΔT_{DC} in $T_p^{\max}$ (due to local heating of the Au lattice), TTM fits to the Au/fused silica data results in similar temperature trends between the determined G_{eff} for Au/fused silica and Au/Si systems. However, we observed a much larger enhancement in G_{eff} for systems with the inclusion of the Ti layer.

range measured in our experiments, the implications of which will be discussed in more detail. The hollow symbols represent data for thicker Au films (40 nm) with Ti adhesion layer. Although the thickness of the Au films for these samples is still below the ballistic length of Au electrons, the measured G_{eff} values are lower compared to the thinner Au films with Ti adhesion layer, the reason for which will also be discussed in the following paragraphs. Furthermore, the substrate dependence for these samples is not as pronounced as for the thinner films.

For the Au films without Ti adhesion layers, the increase in the rate of relaxation due to an increase in laser fluence can be understood as a consequence of increased phase space of the electrons taking part in the scattering mechanisms.[41,54] The absorption of the pump pulse incident on the metal surface creates an electron-hole pair distribution near a narrow region ($\sim 1.5 k_B T_e$) around the Fermi surface. The Pauli exclusion principle dictates that only the electrons in this region are allowed to participate in the energy relaxation process through collisions. Higher fluences leading to higher $T_{e,\text{eff}}$ cause more electrons to take part in the relaxation process that ultimately increases G_{eff}.

The difference between the measured G_{eff} values in the Au films on different substrates with the inclusion of the Ti layer suggests that scattering of the excited Au electrons in the interfacial region (Ti/substrate) plays a role in the enhancement of e-p coupling in these nanosystems. However, we cannot rule out other scattering mechanisms that could be working in tandem to augment heat flow in these systems. For example, the electronic thermal conductance between the Au and Ti layer, h_{ee}, and the electronic thermal conductivity and e-p coupling in each layer in adjunction to metal-electron/interface energy transfer, h_{ei}, could govern thermal transport at these short time scales. Experimental values of h_{ee} on various metal-metal interfaces have shown that the conductances are an order of magnitude larger than the phonon mediated conductances.[55,56] Theoretically, due to this above argument, we can safely neglect h_{ee} as other conductances control the thermal transport in these systems. We experimentally support this assertion later in this section.

At room temperature, the characteristic e-p relaxation length scale is $\sqrt{\kappa_e/G}$, where κ_e is the electronic thermal conductivity. Using a value of 320 W m^{-1} K^{-1} for the electronic thermal conductivity and a value of 3×10^{16} W m^{-3} K^{-1} for e-p coupling in Au yields an e-p mean free path of $\approx$100 nm. Similarly, for Ti, using $\kappa_e = 8.2$ W m^{-2} K^{-1} determined from electrical resistivity measurements[57] and $G = 1.3 \times 10^{18}$ W m^{-3} K^{-1} (Ref. 44), results in a mean free path of $\sim$3 nm. The thicknesses of the bi-layers used in this work (Table I) are less than the e-p mean free paths for the respective metals. For these thin film limits, the effective conductance due to e-p coupling is Gd. Due to the very high value of G in Ti ($G = 1.3 \times 10^{18}$ W m^{-3} K^{-1} at room temperature),[44] the effective e-p conductance in the Ti layer is approximately 3 GW m^{-2} K^{-1}, a value much greater than the effective conductance due to the weak e-p coupling in the Au layer ($\approx$350 MW m^{-2} K^{-1} at low absorbed laser fluences and room temperature conditions). These arguments suggest that the main parameters affecting thermal transport in samples with the thin Ti layers for the short time scales considered in this work are h_{ei} and e-p coupling in the Au layer. The effective e-p conductances in each metal layer are added in series (e-p resistances add in parallel) and therefore with the increase of the Au thickness, the weak coupling in the Au layer decreases the value of the G_{eff} measured for the 40 nm Au films. It is important to note that for a thermally thick Ti layer, most of the energy will be deposited in the Ti layer due to the strong e-p coupling that effectively couples all the energy from the electrons to the lattice vibrations.

In our TTM model, we cannot explicitly deconvolve the various scattering mechanisms associated with electron energy transfer in the Ti interfacial region: i.e., e-e scattering across the Au/Ti interface, e-p coupling in the Ti, and electron-metal/phonon non-metal energy transfer (although we have theoretically ruled out the e-e scattering across the Au/Ti interface, h_{ee}, in our previous discussion, we re-address this with experimental measurement below). Hence, we collectively refer to these three conductive pathways as electron-interface conductance, or h_{ei}, as previously defined. Although we have previously measured G_{eff} for thin Au films,[58] the TTM analysis cannot be applied directly to Ti because of the complicated electronic band structure around the Fermi energy which renders the Drude-based thermoreflectance model inapplicable.[50] However, from Fig. 3, it is clear that if the metal film does not strongly adhere with the nonmetal substrate, the substrate dependence in the e-p coupling no longer exists. To further understand the various scattering mechanisms contributing to h_{ei}, we repeat our measurements for samples with a thin Pt layer instead of the Ti layer between the Au film and the nonmetal substrates. We chose Pt as the e-p coupling factor for Pt has been reported to be similar to the value for Ti (Ref. 59) and also because Pt does not adhere strongly to the nonmetal substrates. Figure 4 shows the thermoreflectance signals for a 40 nm Au/Pt/Si and a 20 nm Au/Pt/Si along with the TTM fits. Similar to the thermoreflectance signal for Au films

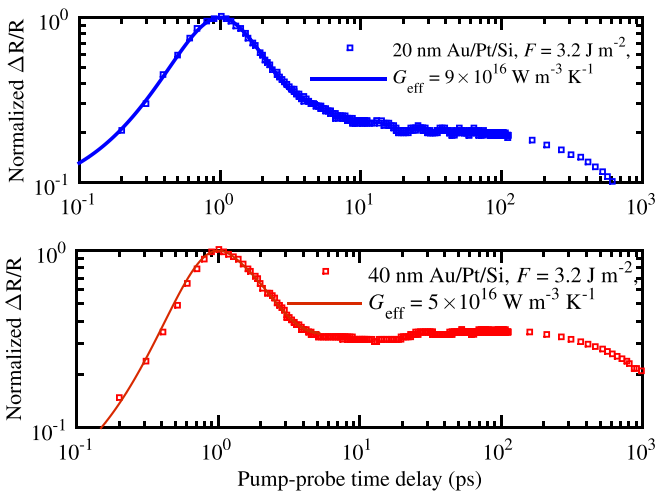

FIG. 4. TDTR data on 20 nm Au/Pt/Si and 40 nm Au/Pt/Si samples with the corresponding fits using the modified TTM with a nonlinear thermoreflectance model for the initial few picoseconds. The thermoreflectance response at longer pump-probe delay times is also shown where the periodic oscillations in the data for 10–100 ps are representative of strain wave propagation.

without the Ti layer, Au/Pt samples also showed the oscillatory signal for delay times of 10–100 ps. This observation is consistent with the fact that the metal films are not strongly adhered to the substrate as the weak bonding allows the strain wave to reflect off the metal/nonmetal interface without pronounced transmission (unlike the case with the Au/Ti samples which will be discussed in more detail in the next subsection). This leads to amplitude modulations in the film thickness due to longitudinal "breathing" of the metal film. The picosecond acoustics has been explained by Tas and Maris[54] from a macroscopic point of view as the propagation of an elastic wave that is launched in the sample due to a thermally induced stress from the laser pulse absorption. As the 20 nm Au/Pt and 20 nm Au/Si samples are heated homogeneously, the thermal stress created at the interface between the film and the substrate generates a thermal expansion of the film due to an elastic wave that reflects at the film/substrate interface.

Contrary to the increase in G_{eff} as a function of electron temperature for samples with the Ti adhesion layer, the e-p coupling in the Au/Pt samples did not show a pronounced dependence on either laser fluence or the different substrates. The predicted G_{eff} values ranged from $8–9 \times 10^{16}$ W m^{-3} K^{-1} and $4–5 \times 10^{16}$ W m^{-3} K^{-1} for 20 nm and 40 nm Au/Pt samples, respectively. These observations suggest that the thermal transport channel in samples with the Ti layer that increases the e-p coupling mechanism is not present in the samples with the Pt layer. Choi *et al.*[55] recently measured the lower limit to $h_{\text{ee}} > 5$ GW m^{-2} K^{-1} across a Au/Pt interface.[55] Therefore, the Au/Pt interface provides negligible resistance (compared to the resistance due to the slow e-p equilibration in the Au layer).

As previously mentioned, we can also rule out electron-metal/phonon non-metal energy transfer in these Au/Pt samples as the metal films are not strongly bonded with the nonmetal interfaces. Therefore, the only resistances to electronic thermal transport in these samples are due to the volumetric e-p coupling in Au and Pt layers. With the knowledge of effective e-p conductance in the Au layer and the total conductance, $G_{\text{eff}}d$, measured by our TTM, we can predict the e-p coupling in the Pt layer as these conductances are added in series. This procedure predicts $G_{\text{eff}} \sim 4–6 \times 10^{17}$ W m^{-3} K^{-1} for Pt which is lower than the previously measured value in Ref. 59. This discrepancy is largely due to the use of a linear temperature dependence of the electronic heat capacity to electron temperature ($C_e = \gamma T_e$) in Ref. 59 for Pt. Whereas, in this work, we use C_e (T_e) values calculated from *ab initio* calculations in Ref. 44 as input parameters in our TTM, the values of which deviate as much as two fold for $T_e \sim 1000$ K from $C_e = \gamma T_e$ with $\gamma = 748$ J m^{-3} K^{-2}.[44]

With these findings, we now revisit our Au/Ti data from Fig. 3. We assert that the measured values of G_{eff} in the Au/Ti films are due to the conductance h_{ei}, which we ascribe as a combination of both e-p coupling in the interfacial Ti layer and e-p conductance across the Ti/substrate interface. Although it is difficult to deconvolute these two conductances to understand the temperature dependence of the hot metal-electron/non-metal phonon thermal boundary conductance, we follow our previous work which predicts "hot" electron-interface thermal boundary conductance. Our model presents a coupled thermodynamic and quantum mechanical derivation of e-p scattering at free electron metal/nonmetal substrate interfaces, the details of which can be found in Ref. 39. Figure 5 shows the model calculations for electron-metal/phonon-nonmetal interactions for the three substrates studied. Calculations are carried out at a lattice temperature of 300 K assuming a Debye approximation for the phonon spectra in each substrate.[60,66,67] The closed symbols and solid lines represent calculations carried out for Au electrons scattering with the various substrates, whereas, the open symbol and dotted lines represents calculations for Ti electrons scattering with the interface. As is clear in Fig. 5, our model predicts linear trends for, h_{es} as a function of electron temperature which is in good qualitative agreement to the trends in the e-p coupling shown in Fig. 3 for samples described in Table I. It should also be noted that the model captures the substrate dependent increase in conductances similar to that in Fig. 3. Based on the discussions from the previous paragraph and the qualitative agreement between our model and the experimental results, heat flow through Au/substrate interfaces could be enhanced through the inclusion of a very thin Ti adhesion layer that allows the electrons to exchange energy with the phonons in the substrate.

This is further supported by the fact that we have ruled out the metal/metal interface as the origin of the linear electron temperature dependence in our data, supporting this hypothesis that the temperature dependence observed in the G_{eff} for the Au/Ti systems in Fig. 3 is due to hot electrons in the metal coupling to vibrations in the substrate. Consequently, we have shown that the presence of a Ti adhesion layer between Au and a dielectric substrate can effectively control heat flow within these nanosystems during e-p nonequilibrium. We note that the substrate dependence in our experimental results could also arise due to the thin Ti layer chemically reacting differently with the various

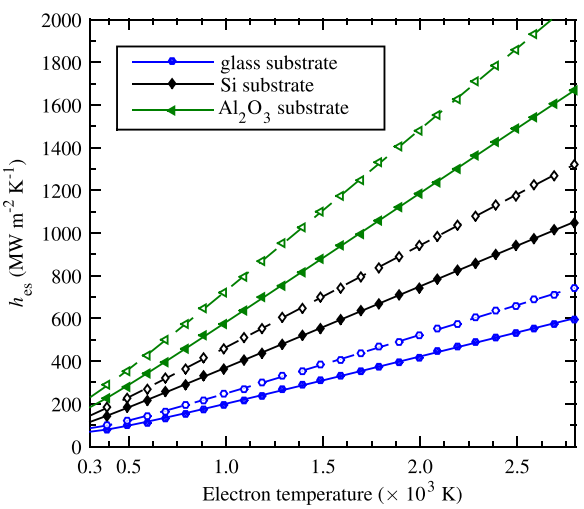

FIG. 5. h_{es} as a function of effective electron temperature for three different substrates at $T_p = 300$ K. The closed symbols represent calculations with parameters for Au electrons, whereas the hollow symbols represent calculations with parameters for Ti electrons. The values of the predicted h_{es} are different for different phonon dispersions of the substrate and are in good qualitative agreement with the conductances measured in Fig. 2 for the samples with the Ti adhesion layer.

substrates, which could in effect change the amount of metallic Ti at the interface. This would lead to a different volumetric coupling between electrons and the Ti lattice for the different dielectric substrates studied in this work. At present, we cannot conclusively rule out this possibility. However, our experimental evidence in Fig. 3 clearly demonstrates the increase in e-p coupling in Au/Ti films compared to Au films, which we attribute to an increased coupling in the interfacial Ti region and/or across the metal/non-metal interface during e-p equilibration.

B. Thermal diffusion processes after electron-phonon equilibration

To further understand the heat distribution and diffusion processes in these nanosystems, we plot the TDTR data for samples with the Ti adhesion layer (on various substrates) for a pump-probe delay time of up to 1 ns in Fig. 6. A qualitative analysis of the magnitude of the TDTR signal over the entire time scale from pump absorption to 1000 ps provides direct insight into the various thermal processes occurring within these temporal regimes in the metal films since the change in the reflectivity measured in our experiments is related to the sample surface temperature. For example, the first few picoseconds after laser absorption is marked by a fast transient decay of the TDTR signal, which we relate to electronic thermalization as described previously. The fast e-p coupling in the Ti layer leads to the increase in the thermal energy of the Ti lattice at a time scale of a few picoseconds after laser pulse absorption (Fig. 2). After the electronic system has equilibrated with the lattice vibrations, at time scales from 10 to 50 ps, the heat has not yet diffused across the metal bi-layer/substrate interface via phonon-phonon mediated transport since energy diffusion due to this process occurs with at least an order of magnitude larger time constant ($\tau_{interface} = dC/h_K$, Ref. 26). Due to the relatively larger time constant for the heat to flow across the metal bi-layer/substrate interface through lattice vibrations, the thermal energy from the Ti lattice is transferred to the relatively colder Au lattice. Consequently, the increase in the temperature of the Au layer leads to an increase in the thermoreflectance signal at these time scales as shown in Fig. 6 for 40 nm Au/Ti systems, similar to the processes discussed in Ref. 55. In comparison to Fig. 1, where the TDTR data at time scales of 10–100 ps are representative of longitudinal displacement of the weakly adhered Au film on the silicon substrate driven by strain induced from the sudden heating event created by the laser pulses,[61] the rise in the thermoreflectivity signal for the samples with the Ti layer suggests that thermal transport in these systems are very different compared to homogeneous thin films. More specifically, thermal diffusion in these Au/Ti samples originates in the interfacial layer between the Au and the substrate due to thermalization of the ballistic electrons that scatter in the Ti layer and at the Ti/non-metal interface. It should be noted that the thermoreflectance signal for the 20 nm Au/Pt sample (as shown in Fig. 4(a)) does not show this increase in the TDTR signal after e-p equilibration even though Pt has a higher e-p coupling factor than Au. This is due to the fact that the effective resistances in each layer due to e-p scattering in the thin film limit, given as $1/Gd$, are comparable, and as a result, the 20 nm Au/Pt system is heated homogeneously. However, for the 40 nm Au/Pt sample, the e-p resistance provided by the Au layer is lower than that in the Pt layer, therefore, there is a slight increase in the thermoreflectance signal from 10–100 ps as shown in Fig. 4(b).

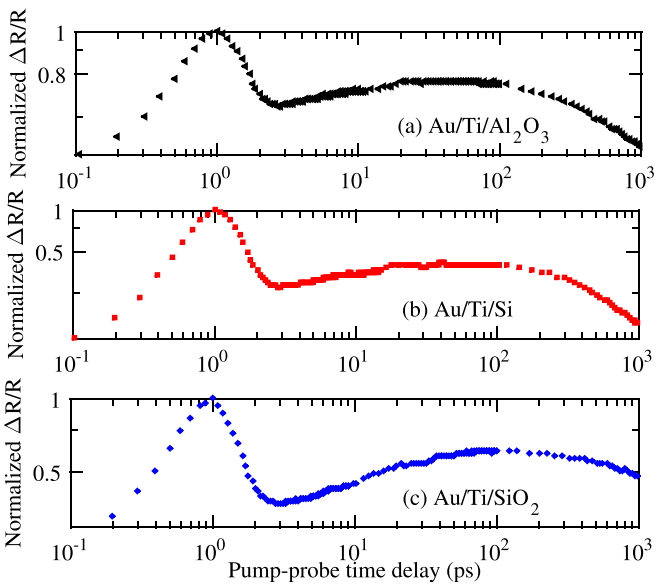

FIG. 6. TDTR data for the initial 1000 ps after laser pulse absorption for (a) 40 nm Au/Ti/Al_2O_3 and (b) 40 nm Au/Ti/Si and (c) 40 nm Au/Ti/SiO_2 The TDTR signal decays rapidly for the first few picoseconds and is related to the electron-phonon coupling process in the thin films. For the 10 to 100 ps time range, samples with the Ti layer show a slow rise in the signal which is attributed to the heating of the Au layer due to heat flow from the Ti layer underneath. This is in contrast to the decreasing TDTR signal (and oscillating picosecond acoustic signal) shown in Fig. 1 for Au deposited directly on Si without a Ti adhesion layer.

These results can help us understand how the increase in e-p coupling due to the Ti adhesion layer affects the total conductance (h_K) across the various Au/Ti/substrate interfaces at longer time scales when the electronic and vibrational states in the metal are in near thermal equilibrium (pump-probe time delays from hundreds of picoseconds to several nanoseconds). We measure the Kapitza conductances for the samples deposited on Si and Al_2O_3 substrates described in Table I by analyzing the TDTR data over a time scale of 100 to 1000 ps. For the Au/Al_2O_3 and Au/Ti/Al_2O_3 samples described in Table I, we measure h_K values of 35 ± 4 MW m^{-2} K^{-1} and 215 ± 15 MW m^{-2} K^{-1}, respectively, and for the Au/Si and Au/Ti/Si samples, we measure h_K values of 88 ± 8 MW m^{-2} K^{-1} and 178 ± 15 MW m^{-2} K^{-1}, respectively. Although h_K measured on this nanosecond time scale demonstrates a large increase with the inclusion of the Ti layer, similar to G_{eff} measured on the picosecond time scale, we do not believe that these two conductance channels are related. For example, if electron-interface scattering from the nonequilibrium regime was influencing our measured h_K, we would expect h_K to vary with G_{eff}, which has both thickness and fluence dependence based on the energy of the hot, ballistically traveling electrons that scatter in the interfacial region. Along these lines, the measured Kapitza conductances for the 40 nm Au/Ti/Sapphire

and 40 nm Au/Ti/Si were within the uncertainties reported for the 20 nm Au/Ti sample, indicating that no thickness dependence is observed in h_K after the electrons and phonons have equilibrated. Also, the TBC for the 40 nm Au/Ti samples showed no fluence dependence suggesting that the electron energy density does not influence the Kapitza conductances for these samples at longer pump-probe delay times ($\sim$1 ns). These observations support the results from previous works that have shown that TBC across metal/nonmetal interfaces are dominated by phonon-phonon mediated processes at the nanosecond time regime.[31,62]

Our results suggest that only at highly nonequilibrium conditions between the electrons and phonons ($T_e \gg T_p$) does h_{ei} contribute to thermal transport for our Au/Ti samples. At time scales when the electrons have completely thermalized with the lattice ($T_e \sim T_p$), h_{ei} does not influence thermal transport.

The improved phonon-phonon conduction at the interface due to the Ti adhesion layer can be attributed to improved bonding between the film and the substrate. Several previous works have demonstrated the increase in phonon-phonon conductance resulting from a stronger interfacial bond between two materials.[40,62–64] In fact, we have previously shown this enhancement in phonon-phonon coupling at 80 nm Au/Ti/Si interfaces compared to Au/Si interfaces, which we analyzed in terms of an increase in adhesion.[62]

In addition to the strengthening of the interfacial bond leading to an increase in the over all h_K, the phonon spectrum in the thin Ti layer could (to a certain extent) play a role in the enhancement of TBC into the substrate. It is well known that a better overlap of low frequency phonon modes can lead to better phonon transmission and an increase in h_K,[65] which the addition of an interfacial Ti layer that has a greater spectral overlap with the Si and Al_2O_3 substrates compared to Au, would produce.

IV. CONCLUSIONS

In summary, we have investigated the role of titanium adhesion layers at the interface of a gold film and non-metal substrate on the rate of electron-phonon energy equilibration. The addition of a $\sim$3 nm Ti adhesion layer increases the magnitude of electron-phonon coupling by as much as a factor of five. By studying systems with different substrates having varying thermal effusivities and phonon dispersions, we show that this enhanced conductance can be attributed to ballistic electrons in the Au coupled to phonons in the interfacial region. We attribute this coupling to either electron-phonon scattering in the thin Ti layer or electron-phonon scattering across the metal/non-metal interface. Moreover, we find that at elevated electron and lattice temperatures, the electron-phonon coupling increases due to an increase in the electron-electron scattering. By analyzing the full temporal regime of the TDTR data from pump absorption to 1 ns, we relate the ballistic electron transport and electron-phonon coupling to the diffusive thermal conductance after electron-phonon equilibrium. This diffusive transport process occurs in two stages: (i) energy deposited in the Ti interfacial region flowing "back" and heating up the Au film followed by (ii) thermal boundary conductance from the Au/Ti into the non-metal. The inclusion of the Ti layer enhances the Kapitza conductance between the metal films and the dielectric substrates, which we attribute in part to the strengthening of the interfacial bond between the metal film and the substrate and also to the phonon spectrum in the Ti layer, consistent with prior works (Refs. 62 and 65). We conclude that electron-metal/phonon non-metal energy transfer does not influence the Kapitza conductance across metal/nonmetal interfaces when the electrons have fully thermalized with lattice vibrations. Our results suggest that only during highly nonequilibrium conditions between the electrons and phonons ($T_e \gg T_p$) does electron-phonon scattering at an interface contribute to thermal boundary conductance.

ACKNOWLEDGMENTS

This material is based upon work supported by the Air Force Office of Scientific Research under AFOSR Award Nos. FA9550-13-1-0067 and FA9550-15-1-0079. This work was also supported by the Laboratory Directed Research and Development (LDRD) program at Sandia National Laboratories. Sandia National Laboratories is a multiprogram laboratory managed and operated by Sandia Corporation, a wholly owned subsidiary of Lockheed Martin Company, for the United States Department of Energy's National Nuclear Security Administration under Contract No. DE-AC04-94AL85000. P.E.H and A.G gratefully acknowledge Professor D. G. Cahill for fruitful discussions.

[1]R. B. Wilson, J. P. Feser, G. T. Hohensee, and D. G. Cahill, Phys. Rev. B **88**, 144305 (2013).
[2]W. Wang and D. G. Cahill, Phys. Rev. Lett. **109**, 175503 (2012).
[3]P. E. Hopkins, L. M. Phinney, and J. R. Serrano, J. Heat Transfer **133**, 044505 (2011).
[4]S. V. Kilina, D. S. Kilin, V. V. Prezhdo, and O. V. Prezhdo, J. Phys. Chem. C **115**, 21641 (2011).
[5]Y. Jiang, H.-Y. Wang, L.-P. Xie, B.-R. Gao, L. Wang, X.-L. Zhang, Q.-D. Chen, H. Yang, H.-W. Song, and H.-B. Sun, J. Phys. Chem. C **114**, 2913 (2010).
[6]M. Kaganov, I. Lifshitz, and L. V. Tanatarov, Sov. Phys. JETP **4**, 173 (1957).
[7]P. B. Allen, Phys. Rev. Lett. **59**, 1460 (1987).
[8]R. W. Schoenlein, W. Z. Lin, J. G. Fujimoto, and G. L. Eesley, Phys. Rev. Lett. **58**, 1680 (1987).
[9]G. L. Eesley, Phys. Rev. B **33**, 2144 (1986).
[10]H. E. Elsayed-Ali, T. B. Norris, M. A. Pessot, and G. A. Mourou, Phys. Rev. Lett. **58**, 1212 (1987).
[11]J. G. Fujimoto, J. M. Liu, E. P. Ippen, and N. Bloembergen, Phys. Rev. Lett. **53**, 1837 (1984).
[12]R. H. M. Groeneveld, R. Sprik, and A. Lagendijk, Phys. Rev. B **45**, 5079 (1992).
[13]S. D. Brorson, J. G. Fujimoto, and E. P. Ippen, Phys. Rev. Lett. **59**, 1962 (1987).
[14]J. Hohlfeld, S.-S. Wellershoff, J. Güdde, U. Conrad, V. Jähnke, and E. Matthias, Chem. Phys. **251**, 237 (2000).
[15]S. D. Brorson, A. Kazeroonian, J. S. Moodera, D. W. Face, T. K. Cheng, E. P. Ippen, M. S. Dresselhaus, and G. Dresselhaus, Phys. Rev. Lett. **64**, 2172 (1990).
[16]M. Mihailidi, Q. Xing, K. M. Yoo, and R. R. Alfano, Phys. Rev. B **49**, 3207 (1994).
[17]P. E. Hopkins, J. C. Duda, B. Kaehr, X. Wang Zhou, C.-Y. Peter Yang, and R. E. Jones, Appl. Phys. Lett. **103**, 211910 (2013).
[18]S. I. Anisimov, B. L. Kapeliovich, and T. L. Perelman, Sov. Phys. JETP **39**, 375 (1974).

[19]C. Thomsen, J. Strait, Z. Vardeny, H. J. Maris, J. Tauc, and J. J. Hauser, Phys. Rev. Lett. **53**, 989 (1984).
[20]C. Thomsen, H. T. Grahn, H. J. Maris, and J. Tauc, Phys. Rev. B **34**, 4129 (1986).
[21]P. E. Hopkins, J. R. Serrano, L. M. Phinney, S. P. Kearney, T. W. Grasser, and C. T. Harris, J. Heat Transfer **132**, 081302 (2010).
[22]A. J. Schmidt, X. Chen, and G. Chen, Rev. Sci. Instrum. **79**, 114902 (2008).
[23]D. G. Cahill, Rev. Sci. Instrum. **75**, 5119 (2004).
[24]E. T. Swartz and R. O. Pohl, Rev. Mod. Phys. **61**, 605 (1989).
[25]D. G. Cahill, W. K. Ford, K. E. Goodson, G. D. Mahan, A. Majumdar, H. J. Maris, R. Merlin, and S. R. Phillpot, J. Appl. Phys. **93**, 793 (2003).
[26]R. J. Stoner, H. J. Maris, T. R. Anthony, and W. F. Banholzer, Phys. Rev. Lett. **68**, 1563 (1992).
[27]R. J. Stoner and H. J. Maris, Phys. Rev. B **48**, 16373 (1993).
[28]M. L. Huberman and A. W. Overhauser, Phys. Rev. B **50**, 2865 (1994).
[29]A. Sergeev, Physica B: Condens. Matter **263–264**, 217 (1999).
[30]A. V. Sergeev, Phys. Rev. B **58**, R10199 (1998).
[31]H.-K. Lyeo and D. G. Cahill, Phys. Rev. B **73**, 144301 (2006).
[32]P. E. Hopkins, J. Appl. Phys. **106**, 013528 (2009).
[33]P. E. Hopkins, J. C. Duda, and P. M. Norris, J. Heat Transfer **133**, 062401 (2011).
[34]P. E. Hopkins and P. M. Norris, Nanoscale Microscale Thermophys. Eng. **11**, 247 (2007).
[35]P. Singh, M. Seong, and S. Sinha, Appl. Phys. Lett. **102**, 181906 (2013).
[36]A. Majumdar and P. Reddy, Appl. Phys. Lett. **84**, 4768 (2004).
[37]P. E. Hopkins, J. L. Kassebaum, and P. M. Norris, J. Appl. Phys. **105**, 023710 (2009).
[38]P. E. Hopkins and P. M. Norris, Appl. Surf. Sci. **253**, 6289 (2007).
[39]A. Giri, B. M. Foley, and P. E. Hopkins, J. Heat Transfer **136**, 092401 (2014).
[40]P. E. Hopkins, ISRN Mech. Eng. **2013**, 682586 (2013).
[41]B. Y. Mueller and B. Rethfeld, Phys. Rev. B **87**, 035139 (2013).
[42]T. Q. Qiu and C. L. Tien, J. Heat Transfer **115**, 835 (1993).
[43]M. Born and E. Wolf, *Principles of Optics*, 7th ed. (Cambridge University Press, 1999).
[44]Z. Lin, L. V. Zhigilei, and V. Celli, Phys. Rev. B **77**, 075133 (2008).
[45]T. H. Geballe and W. F. Giauque, J. Am. Chem. Soc. **74**, 2368 (1952).
[46]L. R. Holland, J. Appl. Phys. **34**, 2350 (1963).
[47]P. M. Norris, A. P. Caffrey, R. J. Stevens, J. M. Klopf, J. James, T. McLeskey, and A. N. Smith, Rev. Sci. Instrum. **74**, 400 (2003).
[48]F. Abeles, *Advanced Optical Techniques*, edited by A. V. Heel (North-Holland Publishing Co., Amsterdam, 1967), pp. 145–188.
[49]P. E. Hopkins, Phys. Rev. B **81**, 035413 (2010).
[50]A. N. Smith and P. M. Norris, Appl. Phys. Lett. **78**, 1240 (2001).
[51]P. E. Hopkins, Appl. Phys. Lett. **96**, 041901 (2010).
[52]P. E. Hopkins and D. A. Stewart, J. Appl. Phys. **106**, 053512 (2009).
[53]A. Schmidt, M. Chiesa, X. Chen, and G. Chen, Rev. Sci. Instrum. **79**, 064902 (2008).
[54]G. Tas and H. J. Maris, Phys. Rev. B **49**, 15046 (1994).
[55]G.-M. Choi, R. B. Wilson, and D. G. Cahill, Phys. Rev. B **89**, 064307 (2014).
[56]B. C. Gundrum, D. G. Cahill, and R. S. Averback, Phys. Rev. B **72**, 245426 (2005).
[57]B. Singh and N. Surplice, Thin Solid Films **10**, 243 (1972).
[58]A. Giri, J. T. Gaskins, B. M. Foley, R. Cheaito, and P. E. Hopkins, J. Appl. Phys. **117**, 044305 (2015).
[59]A. P. Caffrey, P. E. Hopkins, J. M. Klopf, and P. M. Norris, Microscale Thermophys. Eng. **9**, 365 (2005).
[60]For calculations, we used transverse and longitudinal velocities of 3740 m/s and 5980 m/s for glass[66] and 6450 m/s and 10890 m/s for Sapphire, respectively.[67] The details of the calculations for Si are given in Ref. 39.
[61]G. Tas and H. J. Maris, Phys. Rev. B **55**, 1852 (1997).
[62]J. C. Duda, C.-Y. P. Yang, B. M. Foley, R. Cheaito, D. L. Medlin, R. E. Jones, and P. E. Hopkins, Appl. Phys. Lett. **102**, 081902 (2013).
[63]P. E. Hopkins, M. Baraket, E. V. Barnat, T. E. Beechem, S. P. Kearney, J. C. Duda, J. T. Robinson, and S. G. Walton, Nano Lett. **12**, 590 (2012).
[64]M. D. Losego, M. E. Grady, N. R. Sottos, D. G. Cahill, and P. V. Braun, Nat Mater **11**, 502 (2012).
[65]R. Cheaito, J. T. Gaskins, M. E. Caplan, B. F. Donovan, B. M. Foley, A. Giri, J. C. Duda, C. J. Szwejkowski, C. Constantin, H. J. Brown-Shaklee, J. F. Ihlefeld, and P. E. Hopkins, Phys. Rev. B **91**, 035432 (2015).
[66]D. G. Cahill, S. K. Watson, and R. O. Pohl, Phys. Rev. B **46**, 6131 (1992).
[67]D. E. Gray, *American Institute of Physics Handbook*, 3rd ed. (McGraw-Hill, New York, 1972).